# TESTING OF THE CIRCLE AND LINE ALGORITHM IN THE SETTING OF MICRO-CT

Alexander Katsevich [1, 2] and Michael Frenkel [1]
[1] iTomography Corp., [2] University of Central Florida (UCF)

*This paper was prepared for presentation at the International Symposium of the Society of Core Analysts held in Snow Mass, Colorado, USA, 21-26 August 2016*

## ABSTRACT

Computed Tomography (CT) image artifacts and long scan times are common problems faced by many micro-CT users. To avoid artifacts, pure circular scanning requires small cone angles leading to longer core scan times. We describe the implementation and present the results of testing on synthetic phantoms and a real core sample of the exact 3D Filtered Backprojection (FBP) algorithm for CT image reconstruction from cone-beam data acquired with the Circle-and-Line (C&L) X-ray source trajectory. The C&L algorithm is fast and eliminates cone-beam artifacts for any cone angle. We show that adding a relatively sparse line scan allows one to both decrease the scan time (by placing circular scans farther apart) and improve image quality. A core example illustrates that a circular scan protocol utilized by a micro-CT scanner can be modified without hardware upgrades to enable the same scanner to collect data sufficient for performing C&L reconstruction.

## INTRODUCTION

Core imaging using cone-beam micro-CT is required to produce images of high quality. The most common source trajectory consists of a sequence of circular scans. Such a trajectory is incomplete, which leads to cone-beam artifacts [1]. To reduce artifacts, micro-CT systems use small cone angle scanning by placing circular scans close to each other, which leads to long scan times. Instead, one can use a helical or Circle-and-Line (C&L) trajectory (both techniques were originally developed for medical CT applications [2-7]). These trajectories are complete and, when coupled with an exact reconstruction algorithm, eliminate constraints on the cone angle. Hence they allow for faster scanning and elimination of cone-beam artifacts. These considerations motivate the use of novel source trajectories and exact reconstruction algorithms for micro-CT imaging of cores.

The case when the source trajectory is a helix is already understood well [8-9]. Less is known about 3D exact reconstruction algorithms and their practical advantages for the C&L trajectories. In this paper, we evaluate the application of the Katsevich FBP image reconstruction algorithm to the C&L trajectory [5-7]. We show that, when compared with circular scanning, C&L allows to improve both the scanner throughput and image quality.

## BRIEF DESCRIPTION OF THE C&L ALGORITHM

Consider a source trajectory consisting of a circle in the plane $x_3 = 0$ and a line. The circle is of radius $R$ and centered at the origin. The line is perpendicular to the plane of the circle and intersects the circle at the point ($R$, 0, 0). The exact FBP algorithm for reconstruction from the cone beam data corresponding to the C&L trajectory was reported in a number of publications [5-7, 10], so here we will describe only its general high-level outline and discuss some of its practical aspects. We will assume that the detector is flat. Let $s$ be the parameter along the source trajectory, $y(s)$ represent the points on the trajectory, $(u,w)$ be the coordinates on the detector (along the row and along the column, respectively), and let $g(s,u,w)$ denote the cone beam data. We assume that the (virtual) detector contains the axis of rotation. The main steps of the algorithm are as follows (cf. [11-12]):

1. Derivative at constant direction: $g_1(s,u,w) = \frac{d}{ds} g(s,u(s,\Theta),w(s,\Theta))$. Here $u(s,\Theta), w(s,\Theta)$ are the detector coordinates of the point where the ray $y(s)+t\Theta$, $t>0$, hits the detector. See [13] for a simple, yet high-resolution algorithm for computing this derivative.
2. Length correction weighting: $g_2(s,u,w) = (1+(u^2+w^2)/R^2)^{-1/2} g_1(s,u,w)$.
3. Forward height rebinning: $g_3(s,u,\rho) = g_2(s,u,w(u,\rho))$. Here $\rho$ is a variable that parametrizes filtering lines.
4. Filtering: $g_4(s,u,\rho) = \mathrm{H} g_3(s,u,\rho)$, where $\mathrm{H}$ is the Hilbert transform along $u$.
5. Backprojection.

Suppose the region of interest inside the object being scanned fits inside the cylinder

$$x_1^2 + x_2^2 < R_0^2, |\, x_3 \,| < H, \tag{2.1}$$

for some $R_0$, $0 < R_0 < R$, and $H > 0$. The object itself can extend outside $|x_3| < H$.

Let us describe the steps (3), (4), and (5) in more detail. The data on the circle and the line are processed slightly differently. Consider the circle first. In this case filtering is performed along detector rows, so the parameter $\rho$ mentioned in steps (3) and (4) above coincides with the variable $w$. Hence, forward height rebinning is not needed and $g_3 \equiv g_2$. Suppose that the circle is parametrized by $(R\cos s, R\sin s, 0)$, $0 \le s < 2\pi$. Denote

$$\begin{aligned} v^*(s,x) &: = R - (x_1 \cos s + x_2 \sin s), \\ u^*(s,x) &: = \frac{R}{v^*(s,x)}(-x_1 \sin s + x_2 \cos s), w^*(s,x) := \frac{R}{v^*(s,x)} x_3. \end{aligned} \tag{2.2}$$

Here $u^*(s,x), w^*(s,x)$ are the detector coordinates of the point $x$ projected onto the detector. The backprojection step is given by the integral

$$f_c(x) = \frac{1}{4\pi^2} \int_0^{2\pi} \frac{g_4(s,u^*(s,x),w^*(s,x))}{v^*(s,x)} ds, \tag{2.3}$$

where we have used that $\rho = w$.

Next consider the line scan. Now $s$ represents the $x_3$-coordinate of the source on the line. If the source is above (resp., below) the plane of the circle, then $s > 0$ (resp., $s < 0$ ). The extent of the line required for reconstruction is given by

$$|s| \le h_{\max} := 2H/(1-(R_0/R)). \tag{2.4}$$

Pick some $q \in [0, 2\pi)$, and consider the plane through the point $(R, 0, s)$ (which represents the source on the line) tangent to the circle at $(R\cos q, R\sin q, 0)$. Intersection of the plane with the detector gives a filtering line. Thus, for each source position, we obtain a family of filtering lines parametrized by the point of tangency on the circle. Parametrizing filtering lines by the point of tangency leads to singularities as $q \to 0, 2\pi$. So, instead, we define $\rho := \cot(q/2)\sqrt{|s|/(2H)}$. In terms of $\rho$ the family of filtering lines on the detector is given by

$$\begin{aligned} w &= m(\rho)u + w_0(\rho),\ m(\rho) := \frac{\sqrt{2H|s|}}{R}\rho,\ w_0(\rho) := \operatorname{sgn}(s)H\rho^2 - \frac{s}{2}, \\ |\rho| &\le \rho_{\max},\ \rho_{\max} := \sqrt{(h_{\max} - |s|)/(2H)}. \end{aligned} \tag{2.5}$$

For a reconstruction point $x$, compute

$$c_1 = 2(1 - x_1/R),\quad c_2 = |s|(1 - (x_1^2 + x_2^2)/R^2),\quad d := c_1|x_3| - c_2. \tag{2.6}$$

If $d > 0$, the image at $x$ is affected by the cone beam data corresponding to the current source position, so backprojection at $x$ is performed. If $d < 0$, the image at $x$ is not affected by the cone beam data corresponding to the current source position, so backprojection at $x$ is not be performed. Denote

$$\rho_{\pm}^* := -\frac{\operatorname{sgn}(s)}{\sqrt{2H}} \frac{\sqrt{|s|}(x_2/R) \pm \sqrt{d}}{1 - (x_1/R)}. \tag{2.7}$$

The values $\rho = \rho_{\pm}^*$ determine two planes that pass through the current source position and contain the reconstruction point $x$. The existence of two planes implies that there are two filtering lines that pass through the projection of $x$ onto the detector. The backprojection step is then given by the integral

$$f_l(x) = -\frac{1}{4\pi^2} \int \operatorname{sgn}(x_3) \frac{g_4(s, u^*(s,x), \rho_+^*(s,x)) - g_4(s, u^*(s,x), \rho_-^*(s,x))}{v^*(s,x)} ds. \tag{2.8}$$

If $x_3 > 0$, the integral in (2.8) is only over the top portion of the line $s > 0$. If $x_3 < 0$, the integral in (2.8) is only over the bottom portion of the line $s < 0$. For each $x$ the integral is over a finite segment of the line, since $d$ in (2.6) becomes negative if $|s|$ is large enough. As before, $u^*(s,x)$ is the coordinate along the row of the projection of $x$ onto the detector. Finally, the complete reconstruction is given by: $f = f_c + f_l$ (2.9

From the above description it is clear that the per view reconstruction times of our exact C&L algorithm and the well-known FDK algorithm are very similar.

## NUMERICAL EXPERIMENTS

In this section, we present the results of C&L testing with simulated and real core data.

**Phantom 1.** Addition of a line scan coupled with an exact reconstruction algorithm eliminates cone-beam artifacts [5-7]. On the other hand, adding a line increases the overall scan time. Hence, it is of interest to determine the maximal stepsize along the line such that cone-beam artifacts are still under control. To investigate this question we conduct experiments on a synthetic data set with parameters typical of those that occur in micro-CT. Our phantom is a collection of identical uniform balls with the attenuation coefficient 1 and radius 0.8 mm. Their centers are at $(5i_x, 5i_y, 2i_z)$, where $i_x, i_y$ =-1,0,1; and $i_z$ = -8,-7,…,8. We select $R_0$=12.5 mm, $H$=9.56 mm (cf. (2.1)). Radius of the circle $R$ = 50 mm, there are 720 views on the circle. The detector is of size 975x975 pixels, with pixels 27x27 μm.

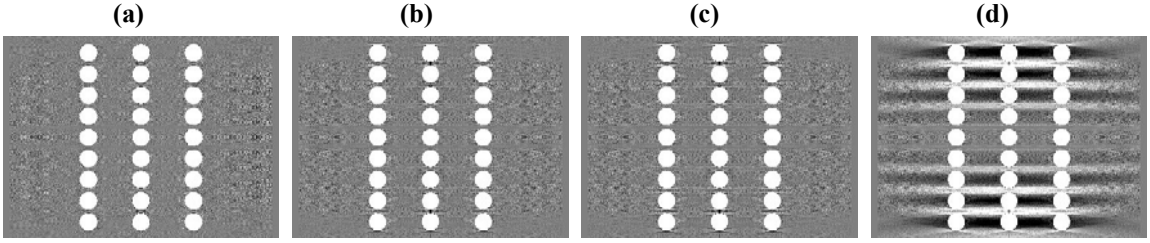


**Figure 1:** Comparisons of C&L (a-c) and Circular (d) reconstructions for cross-section $x_1$=0 mm through the reconstructed Phantom 1. (a), (b), and (c) – 720, 360, and 180 exposures on the line scan, respectively. (d) Circular reconstruction only. Window level: WL=0; window width: WW=0.1; the balls' radii: 0.8 mm.

We conduct three experiments with 720, 360, and 180 sources on the line distributed uniformly over the length of 51 mm. The corresponding reconstruction results for the C&L scan and from only the circular scan are shown in Fig. 1. The images show the region $|x_2| < 12.5$, $|x_3| < 9.56$ mm in the plane $x_1 = 0$ mm. Cone-beam artifacts (dark shadows between and outside the balls) are rather prominent in Fig. 1d, and are practically eliminated in Figs. 1a – 1c. In (d), the artifacts become stronger away from the plane of the circle. Hence, to keep them in check, circular scans need to be close to each other.

Comparing the images in Fig. 1, we see that as the step size on the line gets larger, some discretization artifacts (streaks coming off the tops and bottoms of the balls) get more prominent. Our results suggest that going below 180 source positions (i.e., above the stepsize 0.28 mm) results in noticeable artifacts. However, even with as few as 180 sources on the line, image quality with the line scan is far superior to that with only a circular scan.

**Phantom 2.** Here we choose a collection of small uniform balls. Their radii and centers are selected randomly in the range 0.1-0.3 mm and in the plane $x_3 = 8.14$ mm, respectively. We perform four reconstructions: with 720, 360, and 180 sources on the line and without a line scan. All other parameters remain the same. The results are shown in Fig. 2.

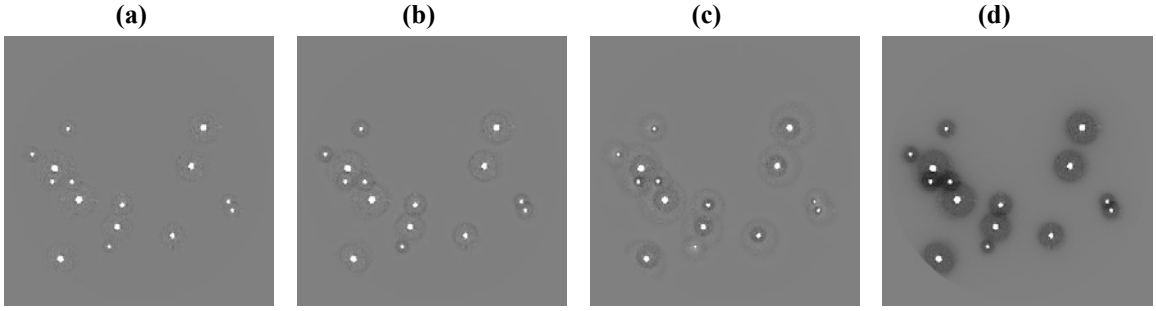


**Figure 2:** Reconstruction results for Phantom 2. (a), (b), and (c) are the C&L images generated for 720, 360, and 180 exposures on the line, respectively; (d) is the Circular reconstruction performed without a line scan. Cross-sections $x_3 = 8.14$ mm for the region: $|x_1| < 12.5$; $|x_2| < 12.5$ mm are shown. WL = 0, WW = 0.1.

As with Phantom 1, cone-beam artifacts (dark halos around white balls) are quite prominent in Fig. 2d. Cone-beam artifacts and discretization artifacts (ripples around the balls) are practically eliminated in Fig. 2a, and become progressively more prominent as sampling of the line scan is reduced. As before, adding even a fairly sparse line scan results in significant image quality improvement.

**Micro-CT imaging of a core sample.** A real core sample (about 8.1 mm in diameter and 7.1 mm tall) was scanned by a micro-CT scanner using a C&L X-ray source trajectory without any hardware changes but by adding a line scan to the circular scan. The source-to-isocenter distance is 25.3 mm, the detector pixel size (at isocenter) is 14x14 μm, and the results of reconstructions are computed on 972x972x550 grid.

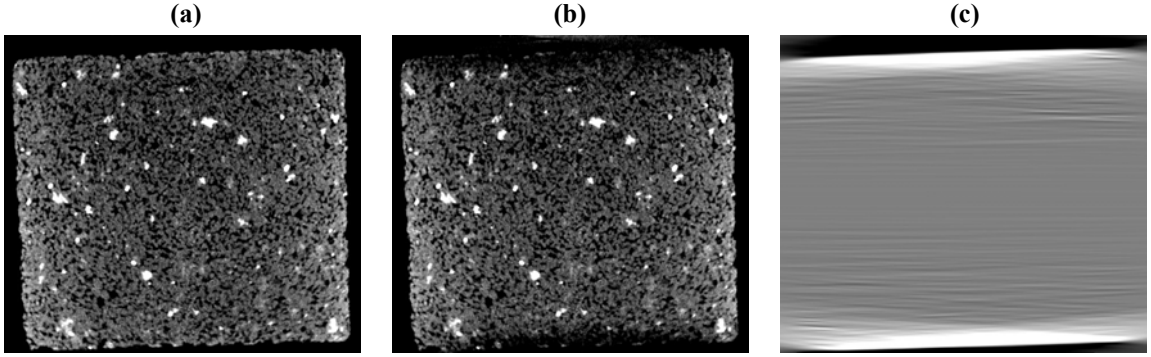


**Figure 3:** Core micro-CT imaging results. (a) C&L and (b) Circular reconstructions (WL = 0.12, WW = 0.1), (c) line contribution (WL = 0, WW = 0.05). Image (a) is the sum of images (b) and (c), see eq. (2.9).

In Figs. 3a and 3b, we present the results of C&L and circular reconstructions for a vertical slice through the core, respectively; the images are of size 972x550. Due to a large cone angle used during the scans (half-cone angle=12º), the top and the bottom parts of the core in Fig. 3b generate strong artifacts masking the image. These parts will have to be cropped out during the subsequent digital micro-CT core analysis. At the same time, the C&L image in Fig. 3a displays perfect image quality for the entire core slice. To better illustrate the artifacts in the circle-only image, in Fig. 3c, we show the reconstruction from the line data. In other words, the image in Fig. 3a is the sum of images in Figs. 3b and 3c.

**Throughput improvement.** Standard circular scan trajectories have to utilize 5-6 degrees half-cone angles to keep cone-beam artifacts below detectable limits [8-9]. In the above experiments with simulated phantom data, we used an 11 degree half-cone angle. This allows for a significant throughput increase, since wider spacing between circular scans makes up for the time used to collect line data. Indeed, our results show that a volume of twice the axial extent can be reconstructed when adding a line scan: 9.5 mm vs. 19 mm. With 720 sources on the circle and one circular scan per every 9.5 mm of axial extent gives for the conventional approach 720/9.5 = 75.8 views/mm. With 720 sources on the circle and one circular scan per every 19 mm of axial extent and with 0.28 mm step size on the line, we get for the C&L approach 720/19 + 1/28 = 41.4 views/mm. This is approximately a factor 1.83 improvement of the throughput (or decrease the scan time by 1.83 times). Similar comparisons of throughput for circular and C&L trajectories can be performed for any micro-CT scanner. It should be noted that 11 degrees half-cone angle was used in this study as a starting point, and C&L works equally well with any higher cone angle [5-7].

## CONCLUSIONS

Noticeable cone-beam artifacts can appear when the source trajectory is a circle or a collection of circles. We show that even with as few as 180 sources on the line, image quality with the C&L scan is far superior to that with only one circular scan. The results presented in the paper indicate that for a given micro-CT scanner it is possible to obtain nearly artifact-free high image quality of cores by utilizing the C&L scan trajectory and application of the Katsevich theoretically exact FBP reconstruction algorithm. Using a real core micro-CT data example, we also illustrate that a conventional circular scan protocol utilized by an existing micro-CT scanner can be modified without hardware upgrades to enable the same scanner to collect C&L data sufficient to perform image reconstruction using the algorithm presented in this paper. C&L allows to use much wider cone angles than those in pure circular scans, which also allows for a significant throughput increase.

## ACKNOWLEDGEMENTS

We would like to thank Igor Frenkel for fruitful discussions regarding the C&L technology.

## REFERENCES

1. Hsieh, J., “Computed Tomography: Principles, Design, Artifacts, and Recent Advances”, *Wiley*, (2009), 510 pp.
2. Katsevich, A., “Analysis of an exact inversion algorithm for spiral cone-beam CT”, *Physics in Medicine and Biology*, **47,** (2002), 2583–2597.
3. Katsevich, A., “Exact filtered back projection (FBP) algorithm for spiral computer tomography”, (2003), US patent **6,574,299**.
4. Katsevich, A., “Improved exact filtered back-projection algorithm for spiral CT”, *Advances in Applied Mathematics*, **32**, (2004), 681-697.

5. Katsevich, A., "Image reconstruction for the circle and line trajectory", *Physics in Medicine and Biology*, **49,** (2004), 5059–5072.
6. Katsevich, A., "Image reconstruction for a general circle-plus trajectory", *Inverse Problems*, **23,** (2007), 2223–2230.
7. Katsevich, A., "Efficient image reconstruction algorithm for the circle and line cone beam computed tomography", (2007), US patent **7,197,105**.
8. Sheppard A., S. Latham, J. Middleton, A. Kingston, G. Myers, T. Varslot, A. Fogden, T. Sawkins, R. Cruikshank, M. Saadatfar, N. Francois, C. Arns, and T. Senden, "Techniques in helical scanning, dynamic imaging and image segmentation for improved quantitative analysis with X-ray micro-CT", *Nuclear Inst. Methods in Physics Res.*, **324,** (2014), 49-56.
9. Katsevich, A., M. Frenkel, M. Feser, Z. Huang, M. Andrew, T. Case, A. Gu, and W. Thompson, "New Fast and Accurate 3D Micro Computed Tomography Technology for Digital Core Analysis", (2015), *SPE ATCE*, Houston, Texas, 13pp.
10. Zamyatin, A., A. Katsevich, and B. S. Chiang, "Exact image reconstruction for a circle and line trajectory with a gantry tilt", *Physics in Medicine and Biology*, **53,** (2008), N423–35.
11. Katsevich, A., K. Taguchi, and A. Zamyatin, "Formulation of four Katsevich algorithms in native geometry", *IEEE Trans. Medical Imaging*, **25,** (2006), 855–868.
12. Noo, F., J. Pack, and D. Heuscher, "Exact helical reconstruction using native cone-beam geometries", *Physics in Medicine and Biology*, **48,** (2003), 3787–3818.
13. Katsevich, A., "A note on computing the derivative at a constant direction", *Physics in Medicine and Biology*, **56,** (2011), N53–N61.